NASA/TM-20210020164

Characterization of Chevron Nozzle Performance

Mark P. Wernet and James E. Bridges
Glenn Research Center, Cleveland, Ohio

October 2021

NASA STI Program . . . in Profile

Since its founding, NASA has been dedicated to the advancement of aeronautics and space science. The NASA Scientific and Technical Information (STI) Program plays a key part in helping NASA maintain this important role.

The NASA STI Program operates under the auspices of the Agency Chief Information Officer. It collects, organizes, provides for archiving, and disseminates NASA's STI. The NASA STI Program provides access to the NASA Technical Report Server—Registered (NTRS Reg) and NASA Technical Report Server—Public (NTRS) thus providing one of the largest collections of aeronautical and space science STI in the world. Results are published in both non-NASA channels and by NASA in the NASA STI Report Series, which includes the following report types:

- TECHNICAL PUBLICATION. Reports of completed research or a major significant phase of research that present the results of NASA programs and include extensive data or theoretical analysis. Includes compilations of significant scientific and technical data and information deemed to be of continuing reference value. NASA counter-part of peer-reviewed formal professional papers, but has less stringent limitations on manuscript length and extent of graphic presentations.

- TECHNICAL MEMORANDUM. Scientific and technical findings that are preliminary or of specialized interest, e.g., "quick-release" reports, working papers, and bibliographies that contain minimal annotation. Does not contain extensive analysis.

- CONTRACTOR REPORT. Scientific and technical findings by NASA-sponsored contractors and grantees.

- CONFERENCE PUBLICATION. Collected papers from scientific and technical conferences, symposia, seminars, or other meetings sponsored or co-sponsored by NASA.

- SPECIAL PUBLICATION. Scientific, technical, or historical information from NASA programs, projects, and missions, often concerned with subjects having substantial public interest.

- TECHNICAL TRANSLATION. English-language translations of foreign scientific and technical material pertinent to NASA's mission.

For more information about the NASA STI program, see the following:

- Access the NASA STI program home page at http://www.sti.nasa.gov

- E-mail your question to help@sti.nasa.gov

- Fax your question to the NASA STI Information Desk at 757-864-6500

- Telephone the NASA STI Information Desk at 757-864-9658

- Write to:
  NASA STI Program
  Mail Stop 148
  NASA Langley Research Center
  Hampton, VA 23681-2199

NASA/TM-20210020164

Characterization of Chevron Nozzle Performance

Mark P. Wernet and James E. Bridges
Glenn Research Center, Cleveland, Ohio

National Aeronautics and
Space Administration

Glenn Research Center
Cleveland, Ohio 44135

October 2021

Acknowledgments

The authors would like to thank Wentworth Trevor John and Garrett Clayo for their efforts related to the setup and installation of the stereoscopic particle-image velocimetry (SPIV) system and for their assistance in performing the data collection. The authors would also like to thank the Aero-Acoustic Propulsion Laboratory (AAPL) staff for their assistance in the operation and maintenance of the experimental rig that produced the results written in this paper. Funding for this work was provided by the Quiet Aircraft Technology (QAT) program at NASA Glenn Research Center.

Level of Review: This material has been technically reviewed by technical management.

Available from

NASA STI Program
Mail Stop 148
NASA Langley Research Center
Hampton, VA 23681-2199

National Technical Information Service
5285 Port Royal Road
Springfield, VA 22161
703-605-6000

This report is available in electronic form at http://www.sti.nasa.gov/ and http://ntrs.nasa.gov/

Characterization of Chevron Nozzle Performance

Mark P. Wernet and James E. Bridges
National Aeronautics and Space Administration
Glenn Research Center
Cleveland, Ohio 44135

Abstract

The flow fields from a set of 50.8 mm diameter circular nozzles were characterized using both streamwise and cross-stream 3-component Stereo Particle Image Velocimetry (SPIV). The test matrix of nozzles included 15 different chevron nozzle designs and one baseline, circularly symmetric nozzle. Nozzle jet operating conditions ranged from acoustic Mach numbers of 0.9 to 1.5, with static temperature ratios ranging between 0.84 and 2.7. Detailed surveys of the single jet flows were performed to capture three-dimensional features of the turbulent exhaust jet evolution. Cross-flow planar measurements were obtained at twelve axial locations, ranging from 0.1 to 20 nozzle diameters downstream of the nozzle exit planes. Streamwise measurements, along the jet centerlines, were obtained at ten partially overlapping downstream locations, providing complete axial surveys over a region extending beyond 20 nozzle diameters downstream of the nozzle exit planes. In both optical configurations, the measurement planes were sized to completely capture the fully turbulent jet shear layer growth. The measured three-dimensional mean and turbulent velocity fields, along with computed second order statistics including axial vorticity and turbulent kinetic energy, were evaluated for all test points. Well-defined streamwise vortex structures in the jet shear layers were measured and reported.

The entire data set of PIV velocity data set discussed in this paper is available (from www.sti.nasa.gov) for those interested in further analysis.

Nomenclature

D	Nominal nozzle diameter, equal to 50.8 mm
L	Length of chevron, measured along jet axis
M_a	Acoustic Mach number, defined as jet velocity divided by ambient speed of sound
$\dot{m}$	Mass flow rate through the nozzle
N	Number of chevrons on nozzle
NPR	Nozzle Pressure Ratio: ratio of the total pressure in the plenum to the ambient pressure
x, y, z	Coordinate axes, referenced to nozzle trailing edge centerline origin, x-axis streamwise
x/D, y/D, z/D	Normalized coordinate axes, referenced to nominal nozzle diameter
u, v, w	Jet velocity components in the x-, y- and z-axes directions, respectively
u′, v′, w′	Fluctuating turbulent components of jet velocity in the x-, y- and z-axes directions, respectively
T_r	Static temperature ratio, defined as ratio of jet static temperature to ambient temperature

1.0 Introduction

Jet noise from turbofan engines is a major contributor to the overall noise levels produced by commercial aircraft. NASA has endeavored for many years to reduce the noise generated by commercial jet engines with the long-term goal of achieving a 20 dB reduction in total perceived aircraft noise. As the primary purpose of the jet is to provide efficient propulsion, any jet noise reduction schemes must not significantly impact the operational performance.

Numerous active and passive methods have been proposed and extensively investigated for jet noise reduction. Active control of jet noise via fluidic injection (Ref. 1) or unsteady actuators (Ref. 2) mounted near nozzle trailing edges have achieved reasonable success through mixing enhancement. These active control techniques have not achieved significant reductions to warrant investigations on how to integrate them into the overall engine hardware. Passive methods, on the other hand, utilize simple geometric modifications to the nozzle itself. Tabs, or small protrusions, located near the trailing edges of nozzles have been utilized to enhance mixing by introducing axial vorticity into the jet shear layers. Although successful at significantly reducing low frequency jet noise, an accompanying penalty has been found in increasing high frequency noise levels (Ref. 3).

Another trailing edge device receiving considerable attention in recent years is the chevron, whose purpose is to introduce longitudinal vorticity into the jet shear layer. This alteration of the mixing layer characteristics has been shown to reduce low frequency noise, albeit to a lesser degree than tabs, but without a significant increase in high frequency content (Ref. 4). Additionally, the chevrons have yielded minimal impact on the aerodynamic performance. The noise characteristics from numerous chevron nozzle designs have been previously investigated at the NASA Glenn Research Center (Ref. 5). An extensive database was generated on far-field acoustics. Additionally, qualitative flow visualization of exhaust plumes using focusing-Schlieren imaging as well as exhaust flow velocity surveys using intrusive pressure and temperature probes were performed. Several exhaust nozzle designs were shown to provide significant jet noise reductions and a <1 percent thrust coefficient reduction under cruise conditions.

These values can be viewed as representative of the baseline noise reduction and thrust preserving potential of the ‘best’ chevron nozzle designs. Further efforts are still necessary to fully quantify and refine the aerodynamic and acoustic performance of the chevron to make it a viable option for widespread installation on more than just a handful of candidate engine nozzle designs. As noted by Thomas et al. (Ref. 6), there is a continuing need to understand and predict jet noise source mechanisms. Significant advances can only be achieved from detailed and accurate measurements of the turbulent velocity fields of the jets. This is particularly true when dealing with relevant high speed, high temperature subsonic jet flows.

SPIV has emerged as a well-suited candidate for providing these measurements, as the technique is not constrained by the limitations of other intrusive methods (Refs. 7 to 9). Furthermore, the types of jet flows produced by chevron nozzles, over a range of nozzle operating conditions similar to those of aircraft takeoff and cruise flight conditions, are well-matched to the measurement capabilities of this technique. Thus, application of SPIV to these types of nozzle exhaust flows is a critical element in arriving at detailed flow-field measurements of three-component velocity, vorticity and turbulence quantities of interest.

This report describes an experimental test program that was undertaken to investigate the relationships between chevron geometry, flow and noise, as described in more detail by Opalski, et al. (Ref. 10). A set of chevron nozzles was designed to parametrically investigate several geometric characteristics deemed important to both flow and noise generation: varying the spacing of axial vorticity through chevron count, varying the strength of axial vorticity through chevron penetration and varying the vorticity distribution within axial vortices through chevron length. Through a detailed examination of these relationships, including far field acoustics measurements, exhaust plume thermocouple and pressure rake surveys, and SPIV measurements, it is anticipated that an excellent set of test cases can be established to aid in the development of robust noise prediction codes. The purpose of the test program presented here is to illustrate the continuing research efforts directed towards accurate measurement of the turbulent velocity fields of single flow hot and cold jets to be used for enhanced aeroacoustic performance characterization. The objective of this report is to make the data collected during the 2003 test program publicly available via the NASA STI office.

2.0 Experimental Facilities

2.1 Single Jet Rig

All the data presented herein were obtained on the Small Hot Jet Acoustic Rig (SHJAR) located within the Aero-Acoustic Propulsion Laboratory (AAPL) at the NASA Glenn Research Center. Figure 1 shows a photograph of the AAPL, which is a 19.8 m radius geodesic dome with its interior walls covered by sound absorbing wedges providing a near anechoic environment. The SHJAR (Figure 2) is a single flow stream free jet rig capable of operating over a range of Mach numbers up to M = 2 at jet static temperature ratios up to approximately 2.8 for a nozzle with Mach 1 exit condition. The centerline of the nozzle exit of the SHJAR is 3 m above the floor. Vitiated flow heating up to 950 K is provided by an inline hydrogen combustor and supply air is provided by central compressor facilities, permitting continuous operation. The SHJAR is oriented such that the exhaust is directed towards the open doorway of the facility. This arrangement permits unrestricted flow seeding operation without introducing noise interference concerns related to particulate collection systems. Additional details regarding the SHJAR and AAPL can be found in Reference 11.

2.2 Chevron Nozzle Models

The downstream end of the SHJAR is comprised of a 0.5 m long, 152 mm diameter settling chamber to which various nozzle models can be attached. The settling chamber contains a series of flow conditioning screens located 0.46 m upstream of the nozzle entrance plane. A single nozzle model, consisting of a two-piece configuration, was used in this test program. The approach profile for this nozzle mounting hardware contracts sharply before rounding out into a final 5° taper leading into the chevron portion of the nozzle, as shown in Figure 3. This design was suitable for use with readily detachable chevron nozzle end pieces.

The one series of chevron nozzle end pieces used with this hardware and investigated in this test program can be described using the following naming convention: SMC for Simple Metal Chevron. Each of the chevron profiles within the SMC family was machined from identically contoured circular blanks. The nozzle blanks were fabricated with a matching 5° taper over the last 0.8 jet diameters. All chevrons were notched within this tapered section using a wire electrical discharge machine (EDM), leaving 30° beveled edges on the chevrons. Alteration of the nominal 5° taper angle was performed by removal of material on the outside base of the nozzles and the careful bending of the chevrons into final position. Removed material was filled back using welding rods.

Previous nozzle chevron studies indicated that high rates of downstream mixing could be generated by the well-spaced low-count chevrons nozzles without the high frequency near-nozzle noise if the clean, 2D shear layers generated by the chevrons could be broken up as they spun up their vorticity. The SMC009 nozzle, which featured 12 chevrons bent in a repeating pattern of 3 chevrons, produced a four-lobed cross-section and centerline decay similar to the SMC001 nozzle which had four large chevrons. The SMC009 nozzle also produced similar low frequency reductions; however, this nozzle did not have nearly as much high frequency penalty. It was also found that, generally speaking, nozzles with more chevrons produced reasonable low frequency benefits without the high frequency penalty, leading to the conclusion that combining high-count chevron designs with a low azimuthal order variation could enhance low frequency reduction.

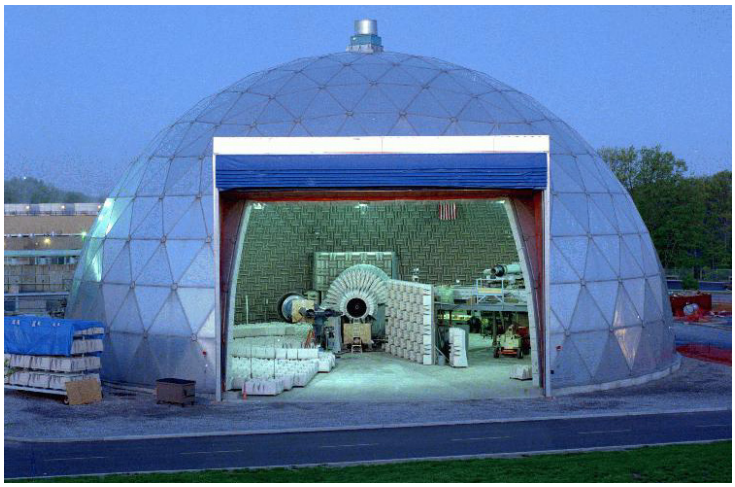

Figure 1.—Photograph of the Aero-Acoustic Propulsion Laboratory.

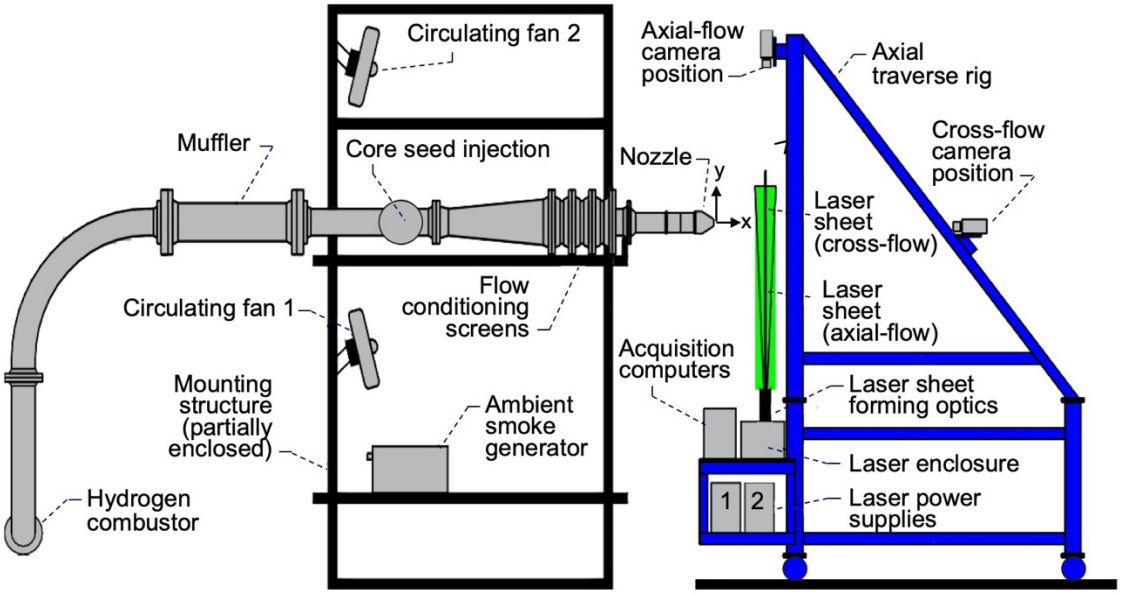

Figure 2.—Layout of the SHJAR and SPIV systems in the Aero-Acoustic Propulsion Laboratory.

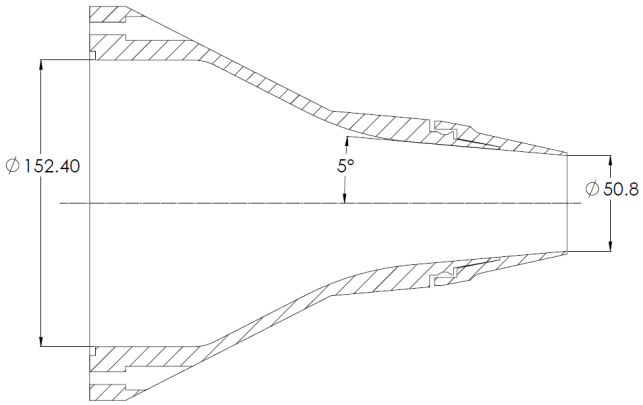

Figure 3.—Geometry of the two-piece mounting nozzle, illustrating the attachment location for different chevron nozzle end pieces. All units are in millimeter.

Three groups of chevron nozzles were developed to accomplish this goal. One, involving azimuthally variations in bending of a high-count chevron nozzle, is called Multi-Scale chevron (MSC) concept. The second approach employs small chevrons on the large flat sides of conventional chevrons and is called the Fractal Chevron (FC) concept. In the FC series of nozzles, the guiding assumption is that increasingly smaller chevrons could be added to the sides of chevrons if the high frequency noise scales on a flow scale more in line with boundary layer or lip thickness than jet diameter. A third concept, more of a diagnostic check on Guiding Principle 2, involves changing the spacing of the axial vortices produced by a chevron nozzle. The two nozzle designs for this concept, dubbed Biased Chevrons (BC), are extremes from a standard chevron design in the spacing of the co-advecting vortex pair produced by a chevron (or more correctly by the notch between chevrons).

In addition to these chevron nozzles, a single pre-machined nozzle from the SMC family, referenced here as SMC000 and shown schematically in Figure 3, served as a baseline circular nozzle profile for this two-piece nozzle configuration. A total of sixteen different chevron nozzle configurations, together with the baseline circular nozzle profile, were investigated in this test program. Photographs of all of the nozzles are shown in Figure 4 and a description of the SMC nozzles can be found in Table 1. The nozzle

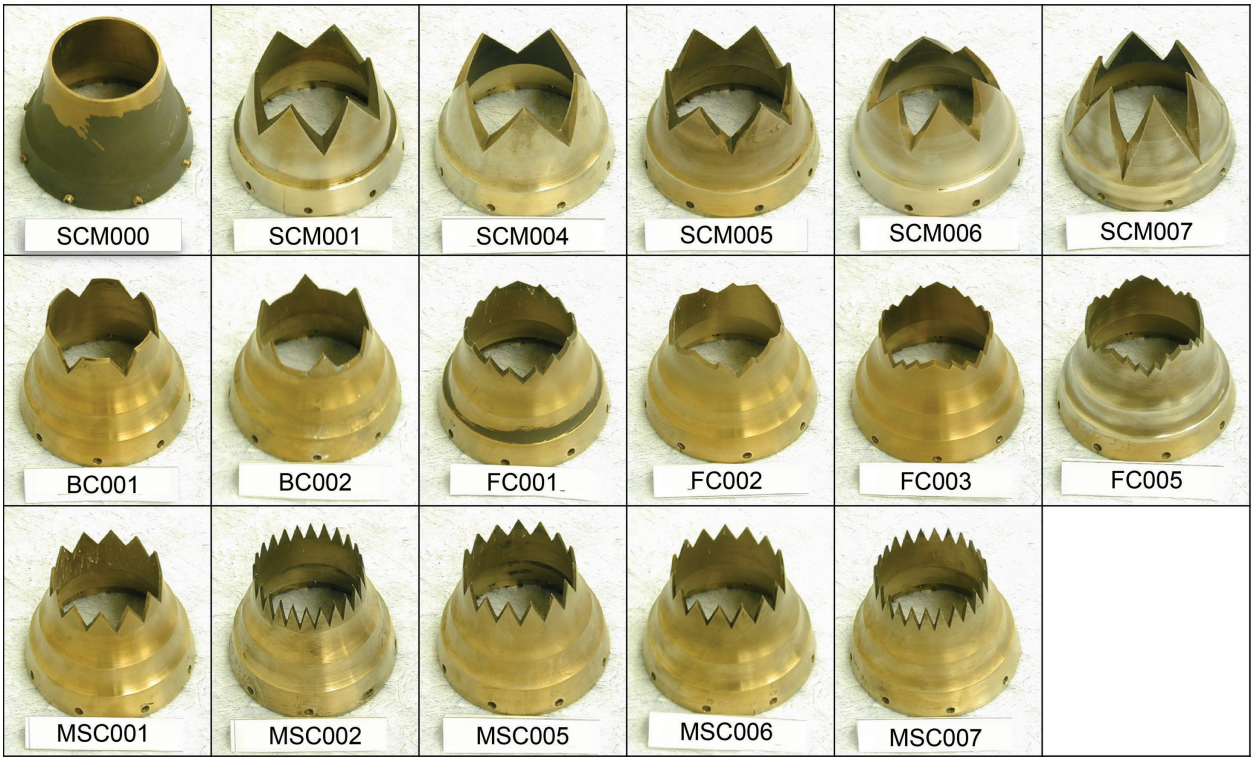

Figure 4.—Photographs of all of the chevron (plus one circular baseline) nozzles used in the test program.

TABLE 1.—DESCRIPTION OF THE SIMPLE METAL CHEVRON NOZZLES USED IN THE TEST PROGRAM

Nozzle identification	Number of chevrons, N	Chevron length, L, mm	Chevron angle, degree	Chevron tip penetration, mm
SMC000	0	-----	----	-------
SMC001	6	22.6	5.0	0.985
SMC004	5	26.6	5.0	1.160
SMC005	6	22.6	0.0	–0.005
SMC006	6	22.6	18.2	3.525
SMC007	6	32.0	13.3	3.681

identification numbers are considered as serial numbers only (order of manufacture) and not meant to distinguish any characterizing feature. In all test cases, the chevron nozzles were mounted in an orientation such that a chevron tip was positioned at top center at the nozzle exit plane. Additional details regarding the design of the SMC family of chevron nozzles can be found in Reference 12 along with a detailed examination of far-field acoustics, thermocouple and pitot-static rake plume surveys of total temperature, total pressure and static pressure of these, and additional chevron nozzle designs.

3.0 Instrumentation/Data Acquisition

3.1 Stereoscopic SPIV System

Stereo PIV systems can be configured in two ways, both cameras on the same side of the light sheet, as depicted in Figure 5, or cameras on opposite sides of the laser light sheet, as shown in Figure 6. Placing the cameras on the same side of the light sheet enables cross-stream PIV measurements of the flow. Placing the camera on opposite sides of the light sheet enables streamwise (axial-plane) measurements. In the cross-flow configuration, there is no alternative set of camera orientations to enable removal of the nozzle from the camera fields-of-view immediately behind the laser sheet, for measurement planes closest to the nozzle. For the axial-flow configuration, the cameras are mounted vertically in the yz-plane rather than horizontally which facilitates the required Scheimpflug condition and avoids having the nozzle in the camera field of view. An additional benefit of orienting the cameras in the yz-plane, is that light from the particles is scattered in the forward direction, resulting in stronger light level signal collection.

The installed SPIV systems consisted of a dual-head pulsed Nd:YAG laser (Continuum Surelite III) operating at 532 nm, and 400 mJ per pulse. The light sheet forming optics consisted of a 1200 mm focal length (FL) spherical lens followed by two cylindrical lenses (–75 and –40 mm FL). The light scattered by particles in the flow was collected by a pair of 2048x2048 pixel cameras (Redlake Megaplus ES 4.0). In the cross-flow measurement configuration, the cameras were positioned at ±40° and equipped with Nikon 135mm f/2.5 lenses combined with 1.4x teleconverters. For the axial-flow measurements, the cameras were oriented at ±45° and fitted with Nikon 105 mm f/2.5 lenses and 2x teleconverters. PCI frame grabbers were used to acquire and stream the image data directly to disk in 200 image-pair sequences (for each camera). Image acquisition occurred at a nominal camera frame rate of ~5 Hz.

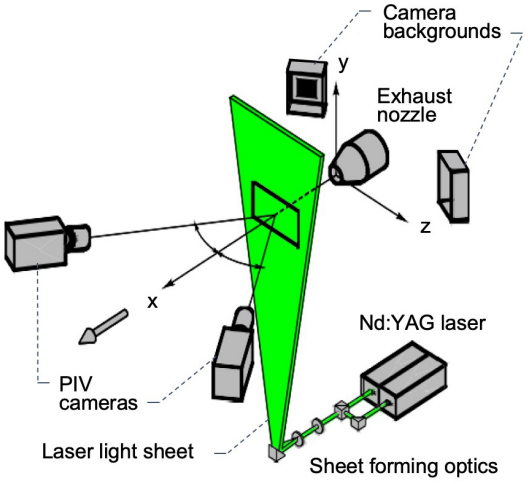

Figure 5.—Experimental arrangement for the cross-flow (perpendicular to jet axis) SPIV measurements.

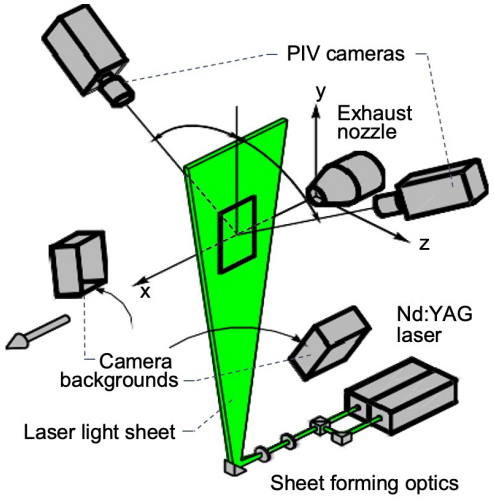

Figure 6.—Experimental arrangement for the axial-flow (parallel to jet axis) SPIV measurements.

Each camera and PCI board was connected to individual dual-processor 3.1 GHz Pentium computers, configured in a Master and Slave mode of operation. The entire system was controlled using NASA developed PIVACQ software. The system was designed and applied to SPIV measurements previously (Ref. 13).

Since the AAPL is open to the environment during testing, the SHJAR could not be operated in complete darkness. To accommodate this situation, optical backdrops for the cameras were provided. These darkened camera backgrounds were positioned such that they were aligned with each camera view behind the measurement plane. The backgrounds were offset a suitable distance to minimize any influence on the ambient seeded flow distribution. Two viable alternatives to aid in reducing ambient light levels, both unavailable at the time of testing, were to either (1) introduce imaging quality laser line filters to the camera lenses, with an accompanying 50 percent attenuation in collected light; or (2) incorporate fast acting shutters in front of the CCD arrays to minimize the duration of the frame-straddled second exposures. This equipment has since been incorporated into the NASA GRC SPIV measurement hardware inventory.

The complete SPIV system, including all cameras and backdrops, data acquisition computers, laser hardware and optics were rigidly mounted on a large axial traverse located downstream of the nozzle exit plane. The travel range of the traverse was approximately 2.5 m, with a positioning accuracy of 1.0 mm. Re-zeroing of the traverse to coincide with the trailing edge of individual chevron nozzles was aided by the installation of a calibration target, required in SPIV, on a fixture secured to the traverse. This enabled highly repeatable cross-flow and axial-flow measurement plane locations with numerous chevron nozzle configuration changes.

3.2 3D Vector Processing

Velocity vector maps for each camera were computed (in the image planes) from the image pairs using NASA developed PIVPROC software (Ref. 14). The software utilizes conventional multi-pass PIV cross-correlation processing algorithms and incorporates error detection based on image correlation signal to noise ratio. First pass interrogation region sizes of 64x64 pixels on 32 pixel centers and final pass interrogation region sizes of 32x32 pixels on 16 pixel centers were used to process image pairs from the cameras in both stereo configurations. For the cross-flow measurement planes near the nozzle, a new PIV data processing technique based upon Symmetric Phase Only Filtering (SPOF) was employed to reduce the effects of flare light on the nozzle models directly behind the measurement planes (Ref. 15). Without the SPOF processing, images with nozzles illuminated by flare light behind the plane of interest generally produce regions in and around the potential core flow with invalid vector measurements. The SPOF processing technique was not utilized with the axial-flow measurement planes as no images with nozzle models in the background were present.

A sample pair of cross-flow configuration raw PIV images is shown in Figure 7. The seeding differences between the nozzle core and the ambient air are readily apparent. Figure 8 shows the results of the combined 3D vector field at the corresponding measurement plane. The color contours represent the out-of-plane w-component of velocity, while the in-plane v- and w-components are shown as vectors. The axes are normalized by the nominal nozzle diameter d = 50.8 mm. Similarly, a sample pair of axial-flow configuration PIV images is shown in Figure 9. Due to the camera rotations required to achieve the Scheimpflug condition in this configuration, the images are rotated 90° with respect to the nozzle flow. Figure 10 shows the results of the combined 3D vector field at the corresponding measurement plane, with the in-plane w-component of velocity contours along with the in-plane u- and v-components shown as vectors. The processed velocity vector maps were approximately 216 by 161 mm in the yz-plane for the

cross-flow configurations and roughly 155 by 127 mm in the xy-plane for the axial-flow configurations. The final resolutions for the processed three-dimensional vector fields in the fluid plane are 1.58 mm for the cross-flow planes and 1.17 mm for the axial-flow planes. Typically, the velocity fields consisted of over 14,000 vectors, for both optical configurations. Ensemble averaging of the 200 individual vector maps was performed to obtain statistical information at each measurement plane. The averaging procedure incorporated both hard velocity cut-off limits and Chauvenet's criterion for data outlier removal (Ref. 16).

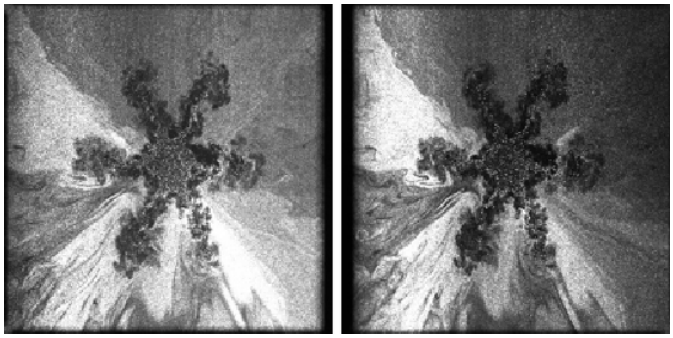

Figure 7.—A typical instantaneous image pair in the cross-flow (yz) plane at x/D = 1.0, for the SMC006 chevron nozzle at M_a = 1.5 and T_r = 2.7 (Set Point 49). Uniform seeding of the core and ambient air can be readily seen.

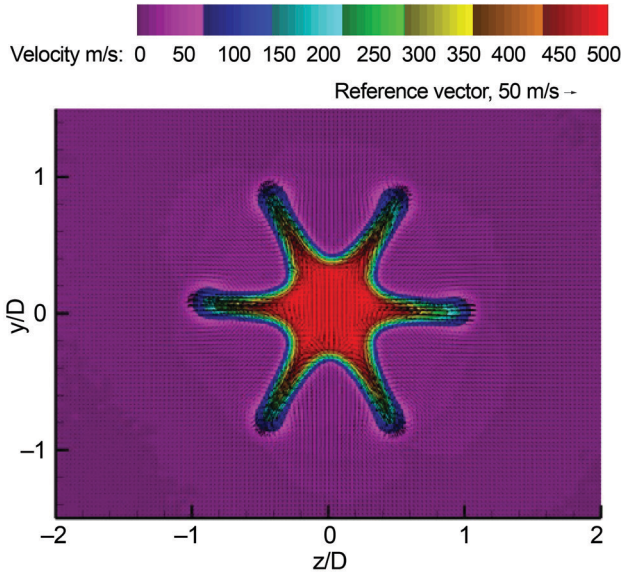

Figure 8.—The ensemble averaged out-of-plane (w-component) velocity contours along with in-plane velocity vectors in the cross-flow plane at x/D = 1.0 for M_a = 1.5 and T_r = 2.7 (Set Point 49). The chevron nozzle is SMC006.

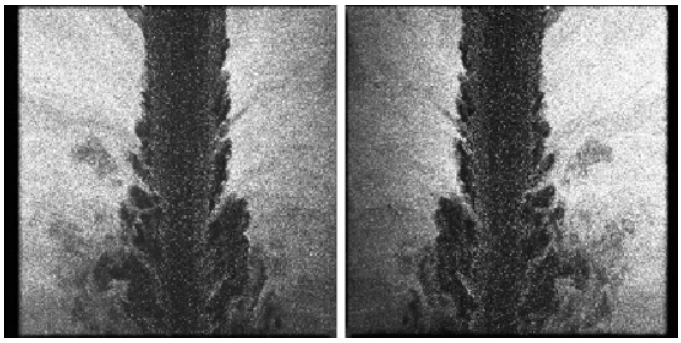

Figure 9.—A typical instantaneous image pair in the axial-flow (xy) plane centered at x/D = 1.20, for the SMC006 chevron nozzle at M_a = 1.5 and T_r = 2.7 (Set Point 49). The potential core flow direction is from top to bottom in these images.

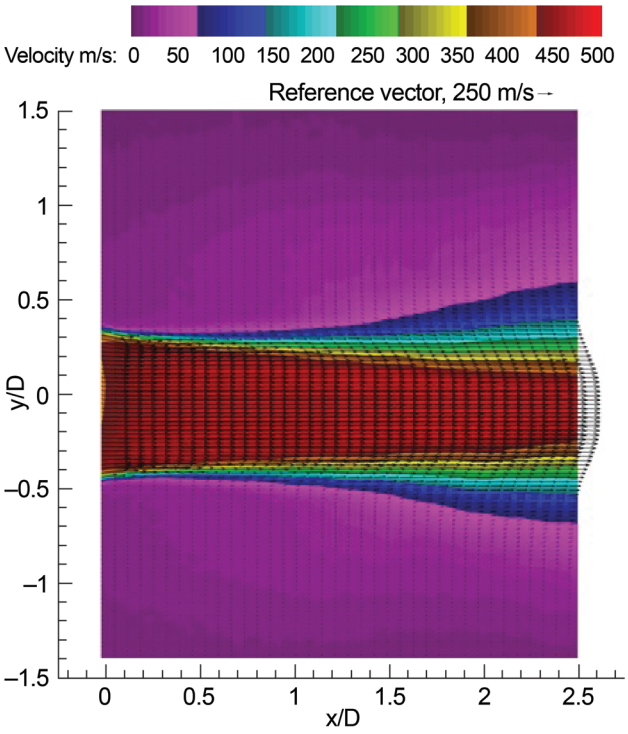

Figure 10.—The ensemble averaged streamwise (u-component) velocity contours along with in-plane velocity vectors (only 20 percent shown for clarity) in the plane centered at x/D = 1.20 for M_a = 1.5 and T_r = 2.7 (Set Point 49). The chevron nozzle is SMC006.

3.3 Flow Seeding

As is typical in all PIV applications, quality flow seeding is essential for obtaining high accuracy results. Due to the elevated operating temperatures, a refractory seed material was required for the core jet flow. The flow seeding material utilized was ~0.5 μm alumina particles. The alumina powder was dispersed in a pH adjusted ethanol solution (Ref. 17) and delivered into the core flow upstream of the flow conditioning screens. Uniform dispersion was provided by a pair of air-assisted atomizing nozzles. As determined from a particle frequency response analysis, the core flow particles were expected to be able to accurately follow the jet flows over the complete range of nozzle operating conditions considered in this test program.

The ambient air was seeded with ~0.2 μm mineral oil droplets produced by a commercial smoke generator. This ambient smoke system was located in a partially enclosed rig support structure upstream of the nozzle. Entrainment of the particles around the nozzles was aided by the use of two circulating fans. This provided a very low velocity (< 5 m/s) air stream surrounding the nozzle core jet flows. The performance of this flow seeding arrangement has been previously applied to PIV measurements with successful results (Refs. 11 and 12).

The use of two separate seeding materials, however, was seen to negatively impact the stereoscopic measurements mainly due to a lack of homogeneous seed particle distributions across the flow regions experiencing high levels of shear. The ability to obtain matching displacement peaks in correlation interrogation regions falling across equivalent nozzle shear layer locations (in both the left and right camera image processing views) was hampered by a slight bias in correlation peak detection. This bias was introduced in cross-correlating interrogation regions which contained moderately higher concentrations of the brighter, and slightly larger diameter, core flow particles. For these interrogation regions which encompassed the entire thickness of the shear layer, it was routine for the 3D vector processing to incorrectly match a lower displacement peak left camera vector that was found and mapped with that of a larger displacement peak right camera vector that was found and mapped, or vice-versa. Then the resulting 3D vector estimate normally failed the residual pixel limit and was excluded from the ensemble estimate. The net consequence is that for the measurement locations within a strong shear region, the number of valid 3D vector measurements are reduced.

3.4 Nozzle Operating Conditions

In a continuing effort to maintain consistency with a growing NASA jet noise database, data were acquired over a small range of flow conditions defined by Tanna (Ref. 18) for cold and hot jet flows. A total of six Set Points were covered in the test matrix, as shown in Table 2. Only three of these Set Points, namely Set Points 7, 46 and 49, will be presented here. These Set Points are best viewed as points deviating in Mach number, velocity and static temperature ratio, which can be further defined as follows: (1) Set Point 7 corresponds to an acoustic Mach number $M_a = 0.9$ and a static temperature ratio $T_r = 0.84$; (2) Set Point 46 corresponds to $M_a = 0.9$ and $T_r = 2.7$; and (3) Set Point 49 corresponds to $M_a = 1.5$ and $T_r = 2.7$. For these three points, velocity is held constant in moving from Set Point 7 to 46 (cold to hot) and the static temperature ratio is held constant in moving from Set Point 46 to 49 (both hot, increase in acoustic Mach number). Gasdynamic Mach number, defined as the jet velocity divided by the local speed of sound, is held constant in moving from Set Point 7 to 49.

TABLE 2.—COMPLETE TEST MATRIX

Set Point	M_a	Tr	NPR	$\dot{m}$, lbm/s
3	0.500	0.950	1.197	0.94
7	0.900	0.835	1.860	1.93
23	0.500	1.764	1.103	0.51
27	0.900	1.764	1.362	0.92
29	1.330	1.764	1.899	1.35
46	0.900	2.700	1.227	0.60
49	1.485	2.700	1.704	0.99

Using these three Set Points with the different chevron designs, the importance of certain chevron design parameters could be evaluated with respect to variations in velocity, static temperature ratio and Mach number. Additionally, the degree to which flow conditions at Set Point 7 correspond to those at typical gas-turbine engine run conditions, such as Set Point 49, could be evaluated. Each of these Set Points corresponds to subsonic, shock-free flow conditions, albeit Set Point 49 is acoustically supersonic.

Maintaining the jet operating conditions was critical in obtaining accurate surveys. At each measurement plane, a total of 200 image pairs per camera were acquired over a period of approximately 40 s. With the rig being fully instrumented, and the air supply being equipped with staged control valves, Set Points were held invariant to within 0.5 percent of the nominal value during these data acquisition periods.

For the cross-plane configuration, data were acquired at 12 downstream locations for each test point. These locations, normalized with respect to the nominal nozzle diameter, are given by x/D = 0.1, 0.2, 0.5, 1.0, 2.0, 3.5, 5.0, 6.5, 8.0, 10.0, 15.0, and 20.0. For the axial-plane configuration, data were acquired at 10 downstream locations for each test point, with each plane centered along the jet axis and overlapping the previous by x/D = 0.43, or 22.0 mm. The corresponding centroid locations of each processed data set plane are given by x/D = 1.20, 3.27, 5.34, 7.41, 9.47, 11.54, 13.61, 15.68, 17.75, and 19.82.

Due to the large size of the test matrix, the PIV image sequence acquisitions were limited to 200 frame pairs at each measurement plane in order to conserve facility run time. Additionally, although facility time constraints precluded a completed test matrix of all chevron nozzles at all test points, the final sampling was determined to adequately characterize the chevron nozzle flows. The success of the experimental test program is evident in that over 500,000 images, corresponding to over 2 TB of uncompressed data, were acquired over the course of the measurement campaign, comprising over 930 individual planar Set Point acquisitions.

4.0 Results and Discussion

The features of the jet plumes emanating from the nozzles is characterized by an examination of the mean velocity distributions, as measured from both cross-flow and streamwise setup configurations. Figure 11 illustrates the resulting cross-flow mean velocity field survey results for a single chevron nozzle (SMC006) under Set Point 49 run conditions (M_a = 1.5, T_r = 2.7). Figure 12 illustrates the resulting axial-flow mean velocity field survey results for the same nozzle under the same operating conditions. Both surveys clearly provide detailed views of the shear layer development for this nozzle designed with a high level of chevron penetration. Further examination of the centerline velocity decays from both measurement configurations also confirm good alignment of the traverse with the jet axis nozzle flows. This alignment held true for cold nozzle flow (Set Point 7) run conditions as well.

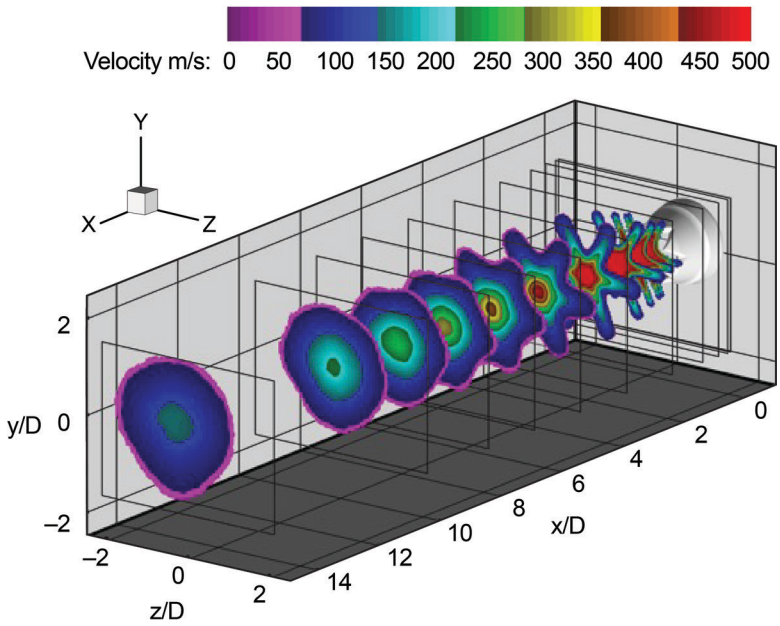

Figure 11.—Cross-plane mean velocity fields at the first 11 (of 12 total) downstream locations for M_a = 1.5 and T_r = 2.7 (Set Point 49) and the chevron nozzle is SMC006.

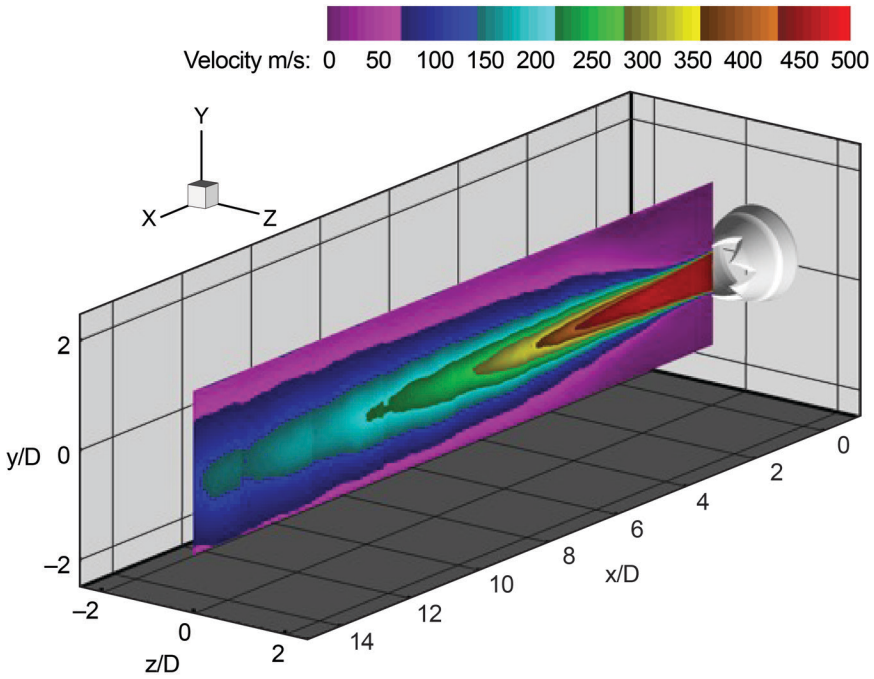

Figure 12.—Axial-plane mean velocity fields along jet centerline at first 7 (of 10 total) downstream locations for M_a = 1.5 and T_r = 2.7 (Set Point 49). The overlap region between planes is x/D = 0.43 and the chevron nozzle is SMC006.

Figure 13 illustrates the mean out-of-plane (w-component) velocity contours, at the first 11 downstream planes, for several of the N = 6 chevron nozzles at Set Point 7 run conditions, compared to the baseline circular nozzle. The different chevron configurations yield unique shear layer patterns in the jet plume. The interesting shear layers developed from these nozzle flows will be examined in further detail below. Figure 14 shows the BC series of nozzles at Set Point 7, where the jet plume is initially observed to be square or triangular near the jet, eventually transitioning to a round plume further downstream. Similarly, the MCC series of nozzles at Set Point 7 are shown in Figure 15. Initially, the jet shear layers have significant spatial variations, which transform into more geometric shapes and eventually transition to round jet plumes further downstream. Figure 16 shows all of the measured nozzles at Set Point 46 and Figure 17 shows all of the measured nozzles at Set Point 49. For the nozzles run at both cold and hot conditions, the reduction in the length of the potential core is readily observed.

Figure 18 to Figure 22 provide turbulent kinetic energy (TKE) measurement profiles from the nozzle and setpoints shown in Figure 13 to Figure 17, calculated using the following expression: $TKE = \frac{1}{2}(u'^2 + v'^2 + w'^2)$. In Figure 18, the dramatic decrease in TKE levels near the end of the potential cores for the SMC nozzles with increasing penetration levels is very evident. Also noticeable is the increase in the TKE levels within the first jet diameter for the increased penetration SMC nozzles. These trends are consistent with and directly correspond to the acoustic observations of decreasing low frequency noise with an accompanying increase in high frequency noise levels, for increasing penetration chevron designs. In Figure 19, the BC nozzles yield lower peak TKE and a faster drop in the TKE than the FC series of nozzles. Comparing the results obtained at Set Point 7 (cold) conditions with those at Set Point 46 (hot), it appears that the hot jets had significantly shorter potential cores for all nozzles. The trend of greater centerline decay with increasing penetration was also maintained throughout the jet profiles, with the largest differences found within the first 5 jet diameters for the hot nozzle flow conditions. In viewing the results obtained at Set Point 46 with those at the higher velocity Set Point 49 (both hot), it is observed that although the extent of the radial ‘arms’ of the high speed regions are greater in the higher velocity jet, the potential core decay rates are very similar.

Figure 23 illustrates plots of axial vorticity for three of the SMC nozzles, an FC and an MSC nozzle at the Set Point 46. The impact of chevron penetration on the development of the jet shear layers in the initial cross-flow planes is clearly evident. Well-defined pairs of counter-rotating vortical structures produced by the opening (notch) between chevrons are clearly seen in the nozzles with large chevron penetrations. The flow results have been aligned from left to right with nozzle geometries having increasing penetration levels. Surprisingly, the differences in vorticity after the first 1.5 jet diameters are small in comparing the nozzles with high (SMC006) and moderate (SMC001) penetrations. This is an indicator that the focus of relevant mixing phenomena analyses should emphasize measurement planes contained within the first 1-2 jet diameters downstream of the nozzle exit planes. The FC and MSC nozzles show much smaller scale vortical strictures which still die out within 2 nozzle diameters downstream.

While not readily apparent in the mean out-of-plane velocity contours, the vorticity distribution surrounding the lip line from the SMC000 baseline nozzle is not axisymmetric as would be expected, and thus requires some further examination. A mismatch between mapped left and right vector fields in the vertical (y-axis) direction appears clear in looking at the raw velocity vector maps, attributed to some combination of left and/or right camera motion to shift the fields-of-view from their initial calibration target views. While no attempt has been made yet to correct for this discrepancy, as previously mentioned, similar mismatches do not appear to materialize in as strong a fashion in the other three nozzle flows, at this Set Point. This leads to the observation that the mismatch becomes greatly amplified in regions of high shear.

The results from all axial-flow measurement planes are presented in Figure 24 (Set Point 7) and Figure 25 (Set Point 49) for the SMC000, SMC005, SMC001, and SMC006 nozzles. Direct comparison of both data sets show that the hotter jets have much shorter potential core regions than their respective cold jets, for all nozzles considered. A potential core length reduction of more than 40 percent (for a 50 percent peak centerline velocity fall-off) was typically seen, which compares very favorably with equivalent measurements obtained from the cross-flow SPIV configuration.

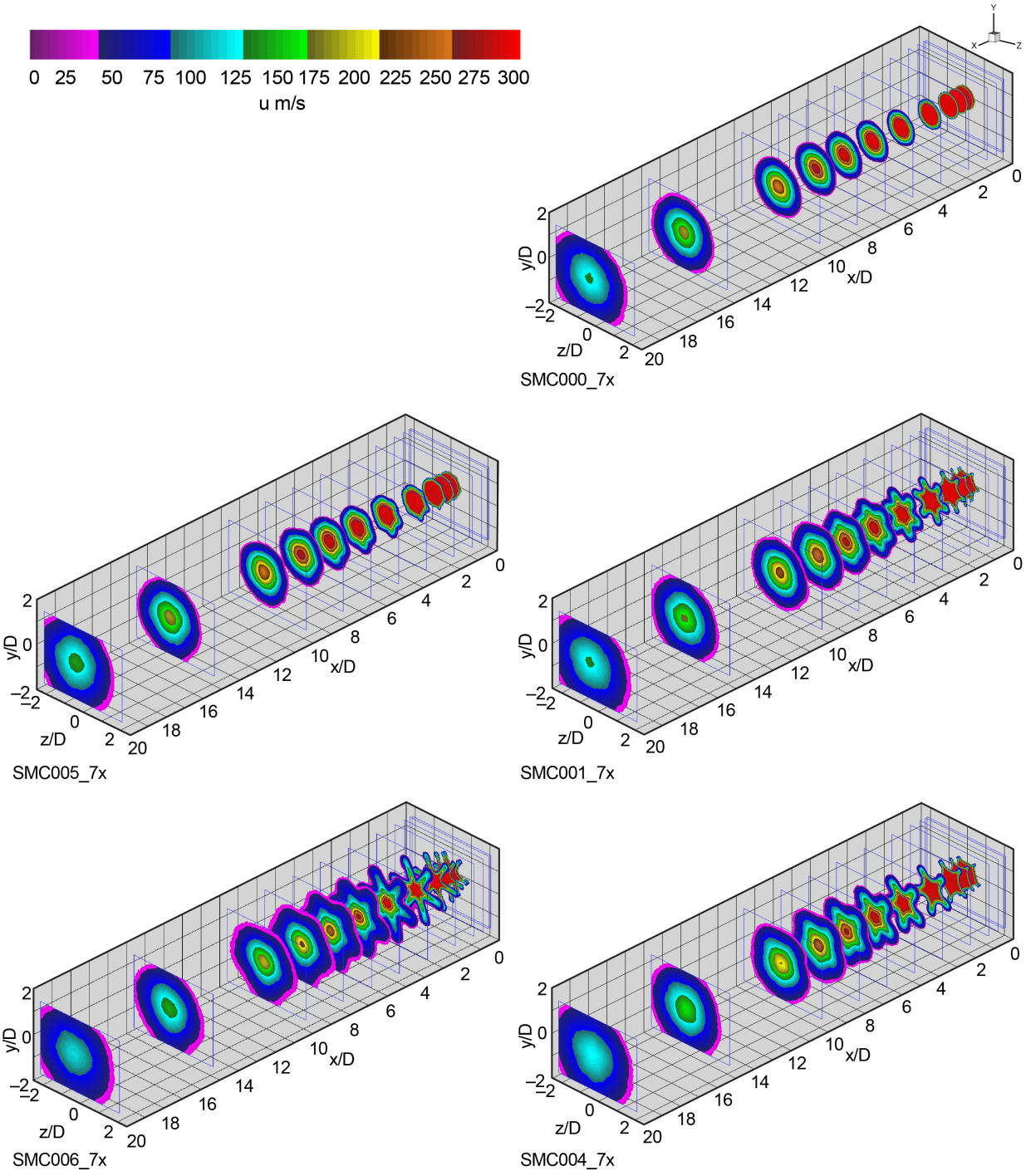

Figure 13.—Contours of the u-component of velocity for SMC series of nozzles at Set Point 7.

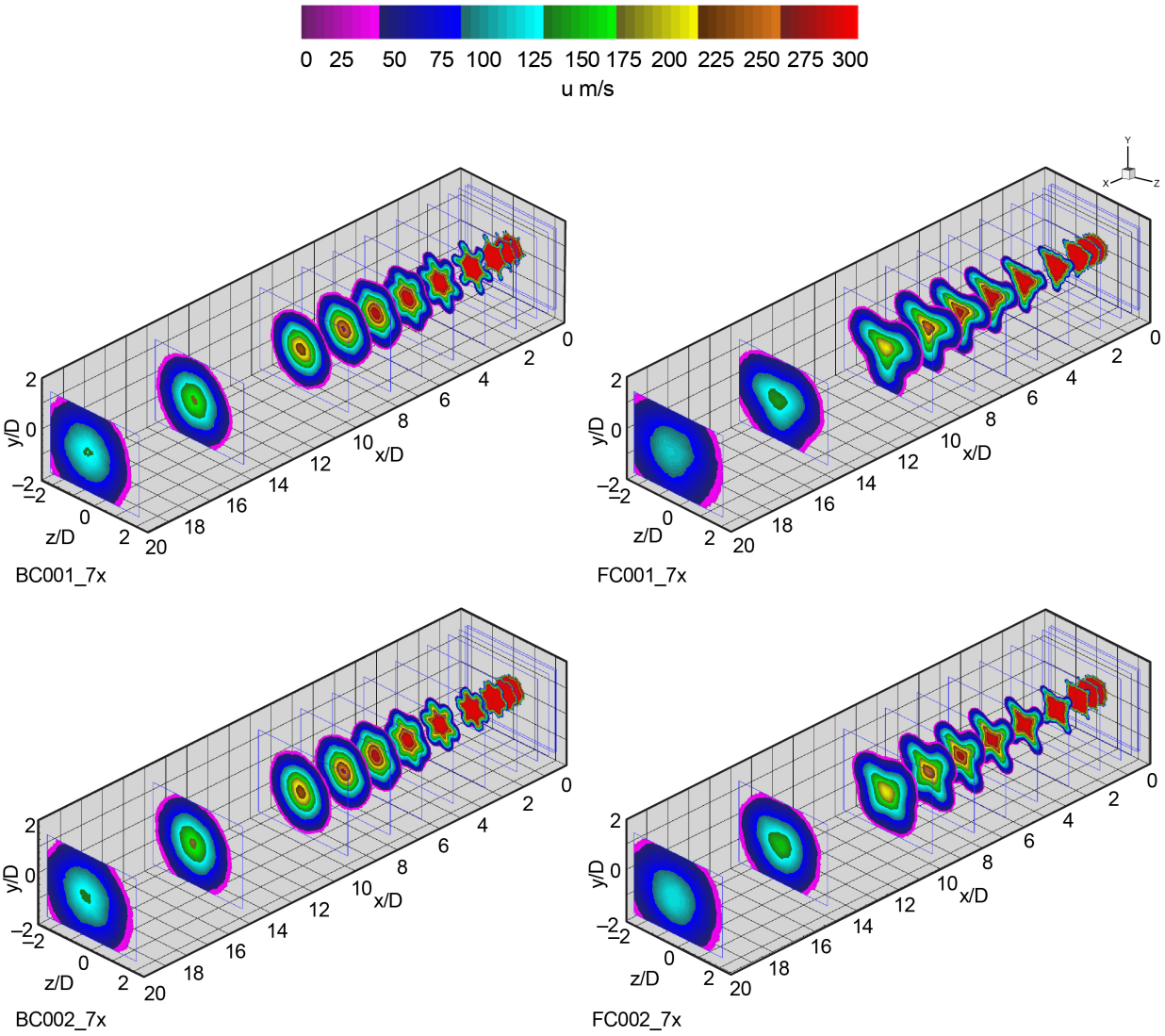

Figure 14.—Contours of the u-component of velocity for BC and FC series of nozzles at Set Point 7.

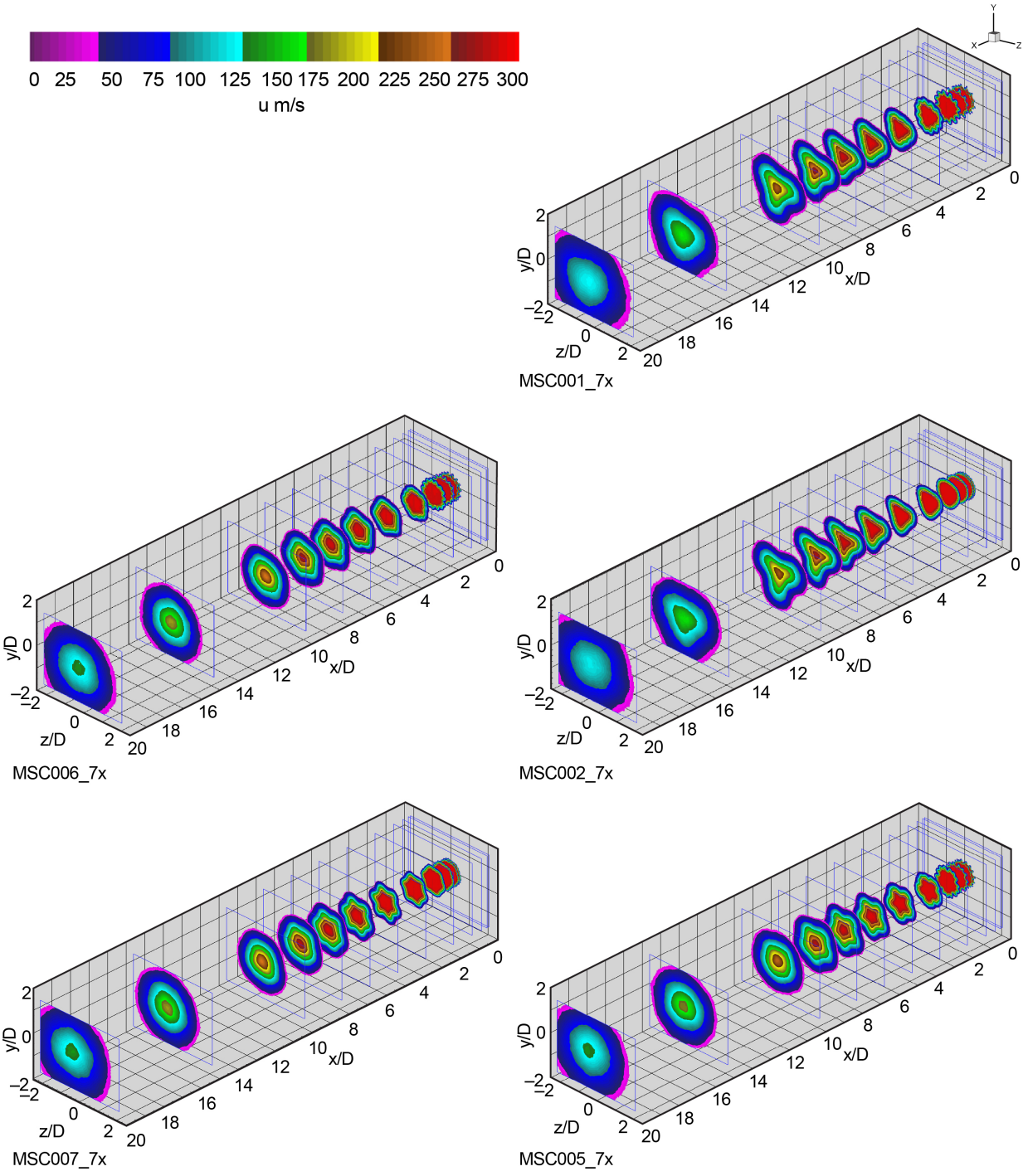

Figure 15.—Contours of the u-component of velocity for MSC series of nozzles at Set Point 7.

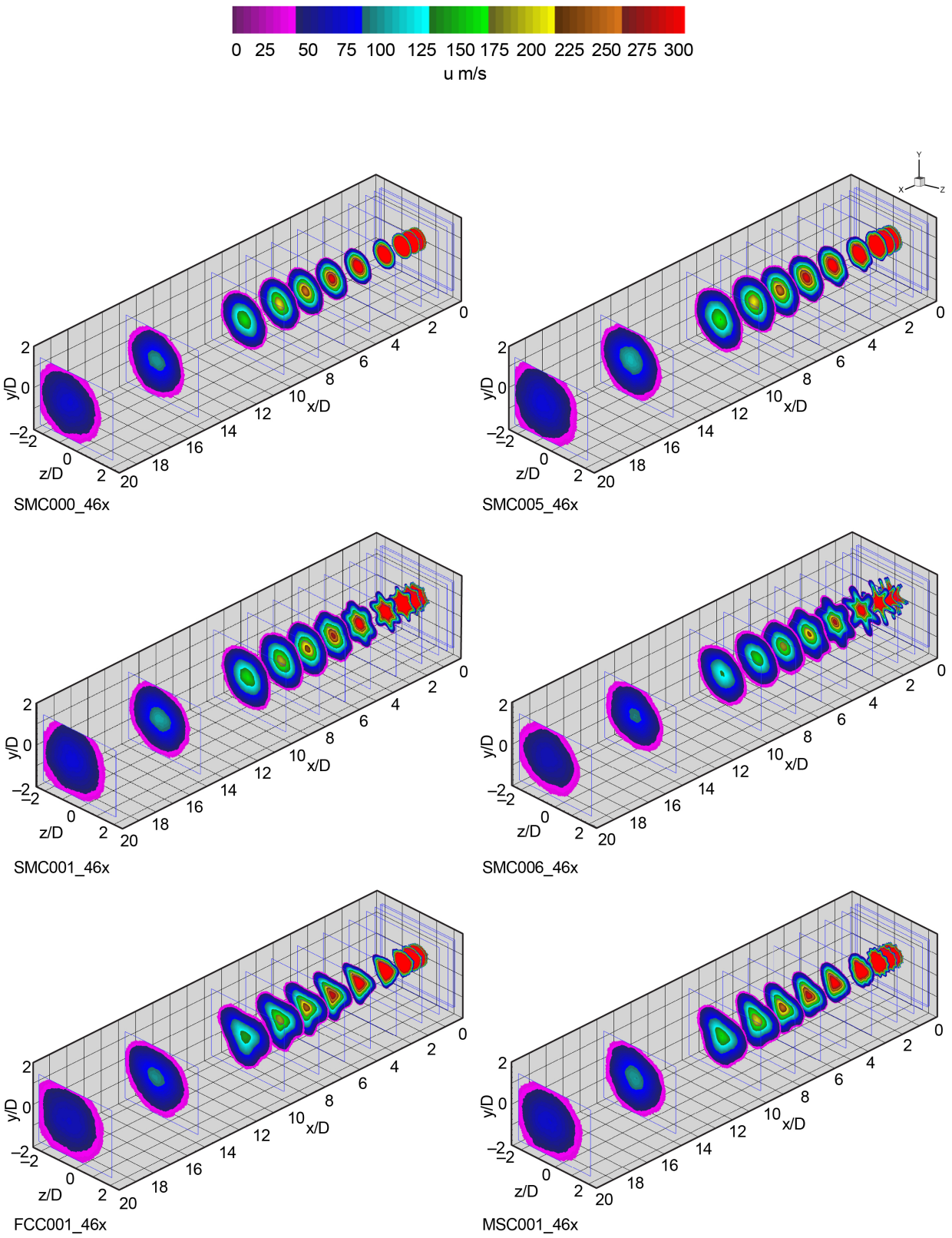

Figure 16.—Contours of the u-component of velocity for SMC, FC and MSC nozzles at Set Point 46.

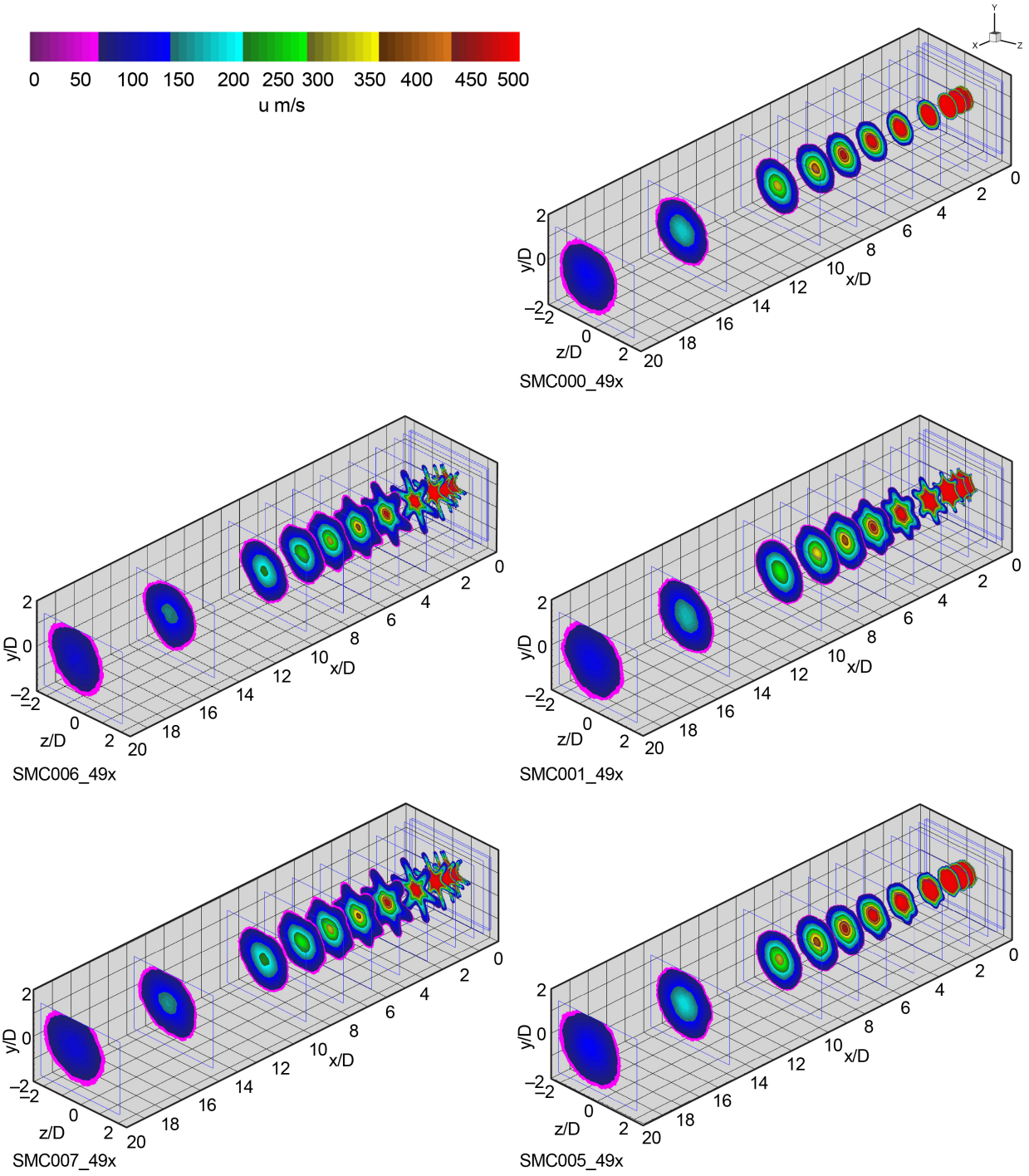

Figure 17.—Contours of the u-component of velocity for SMC series of nozzles at Set Point 49.

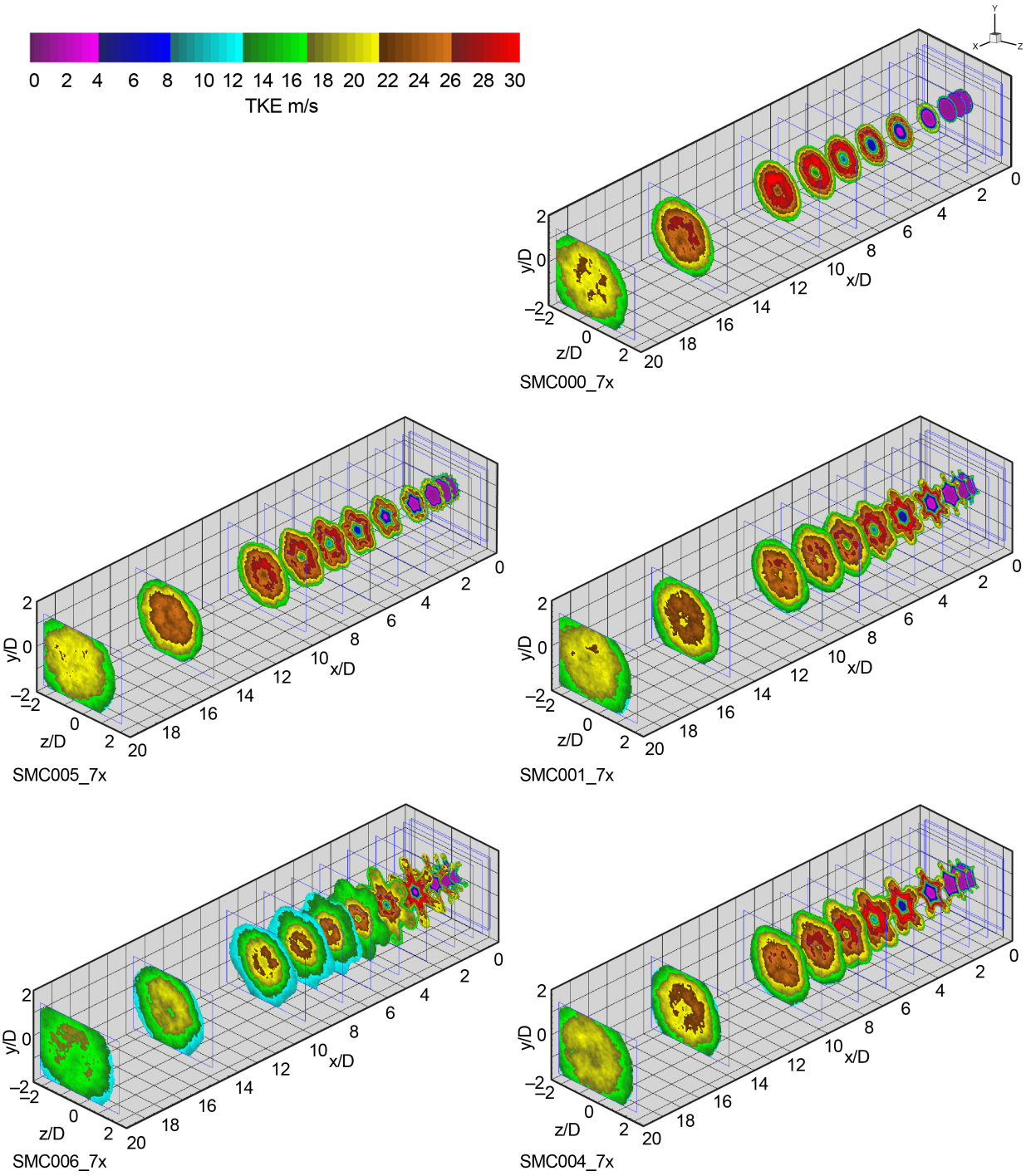

Figure 18.—Contours of TKE for SMC series of nozzles at Set Point 7.

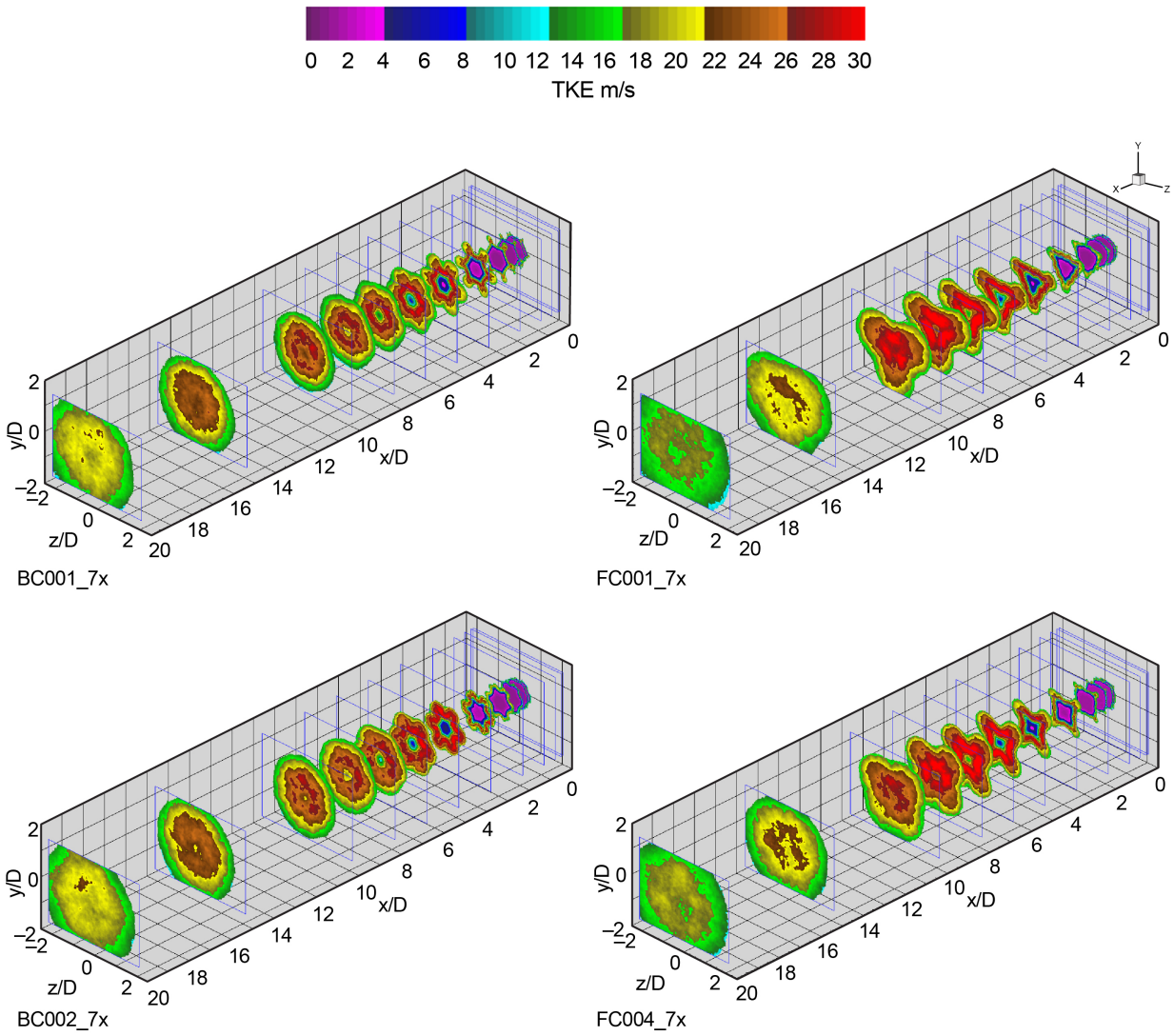

Figure 19.—Contours of TKE for BC and FC series of nozzles at Set Point 7.

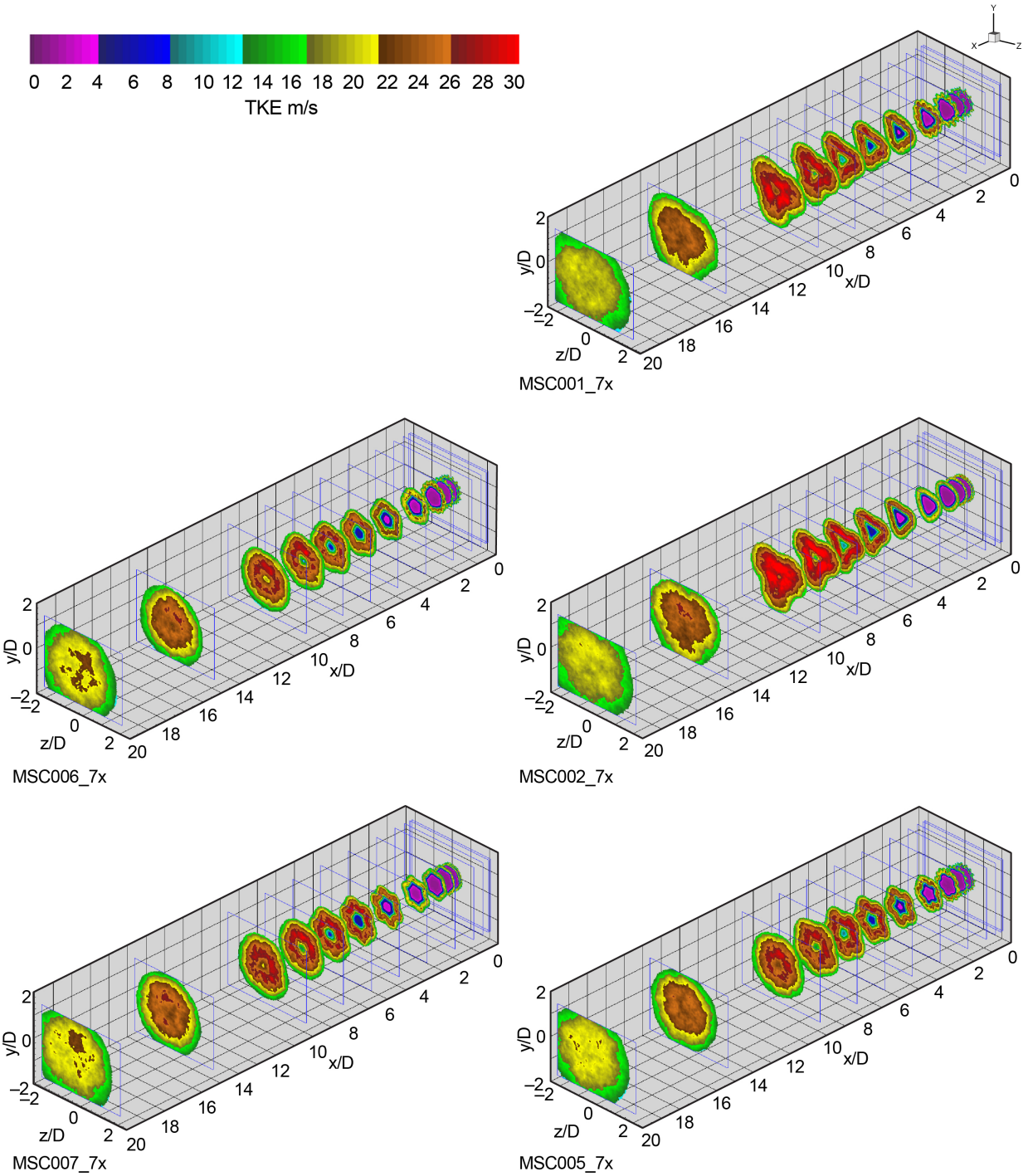

Figure 20.—Contours of TKE for MSC series of nozzles at Set Point 7.

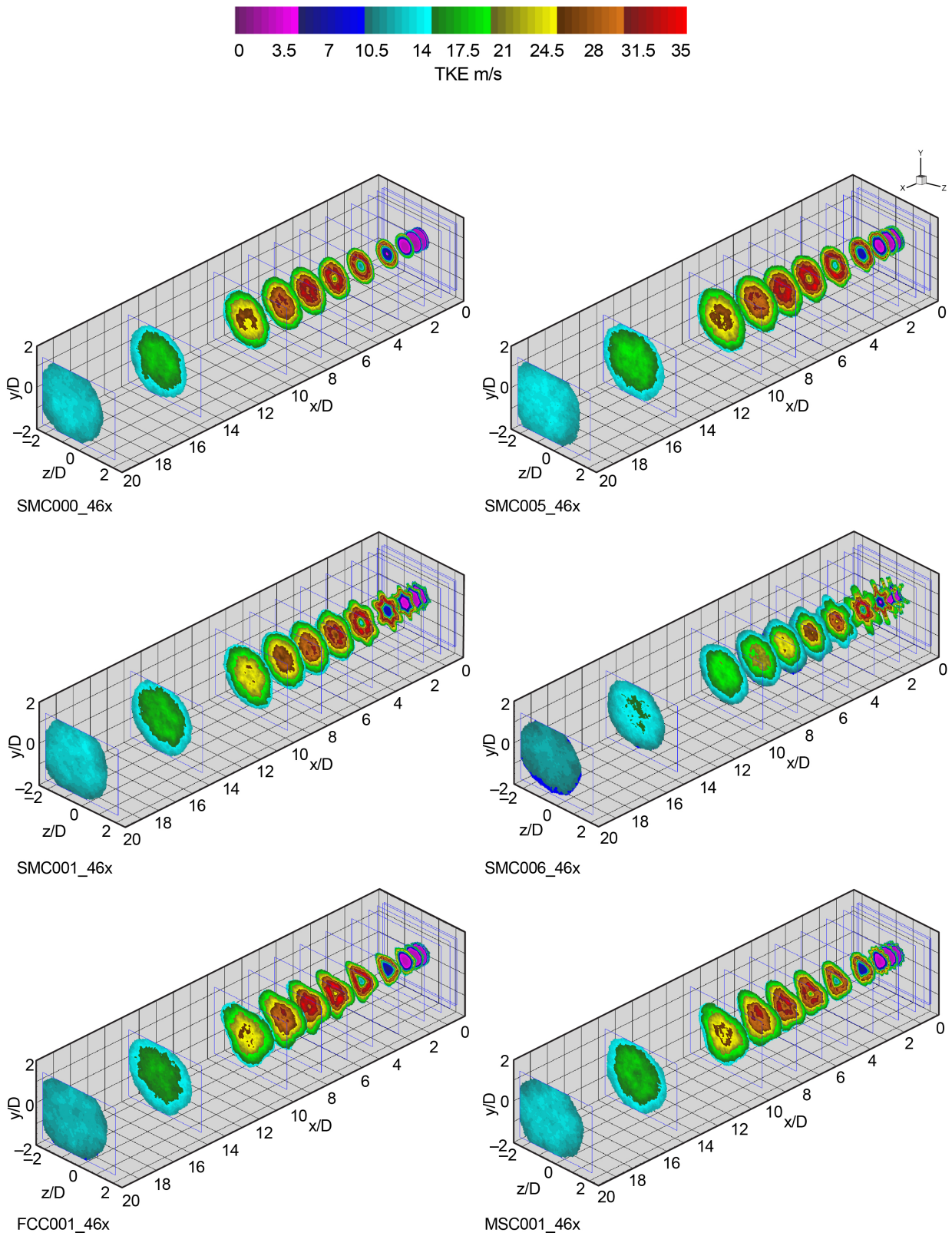

Figure 21.—Contours of TKE for SMC, FC and MSC nozzles at Set Point 46.

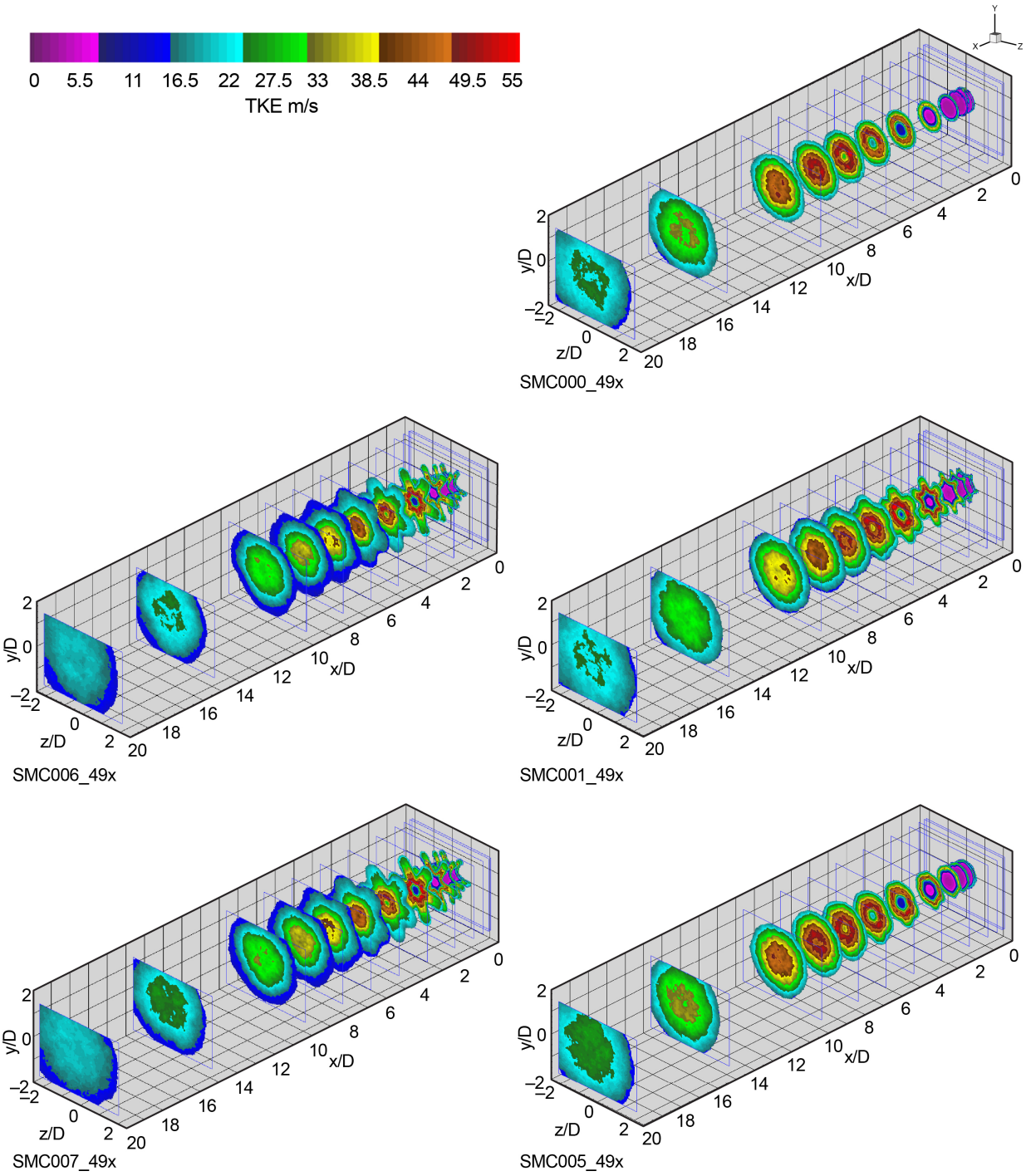

Figure 22.—Contours of the w-component of velocity for SMC series of nozzles at Set Point 49.

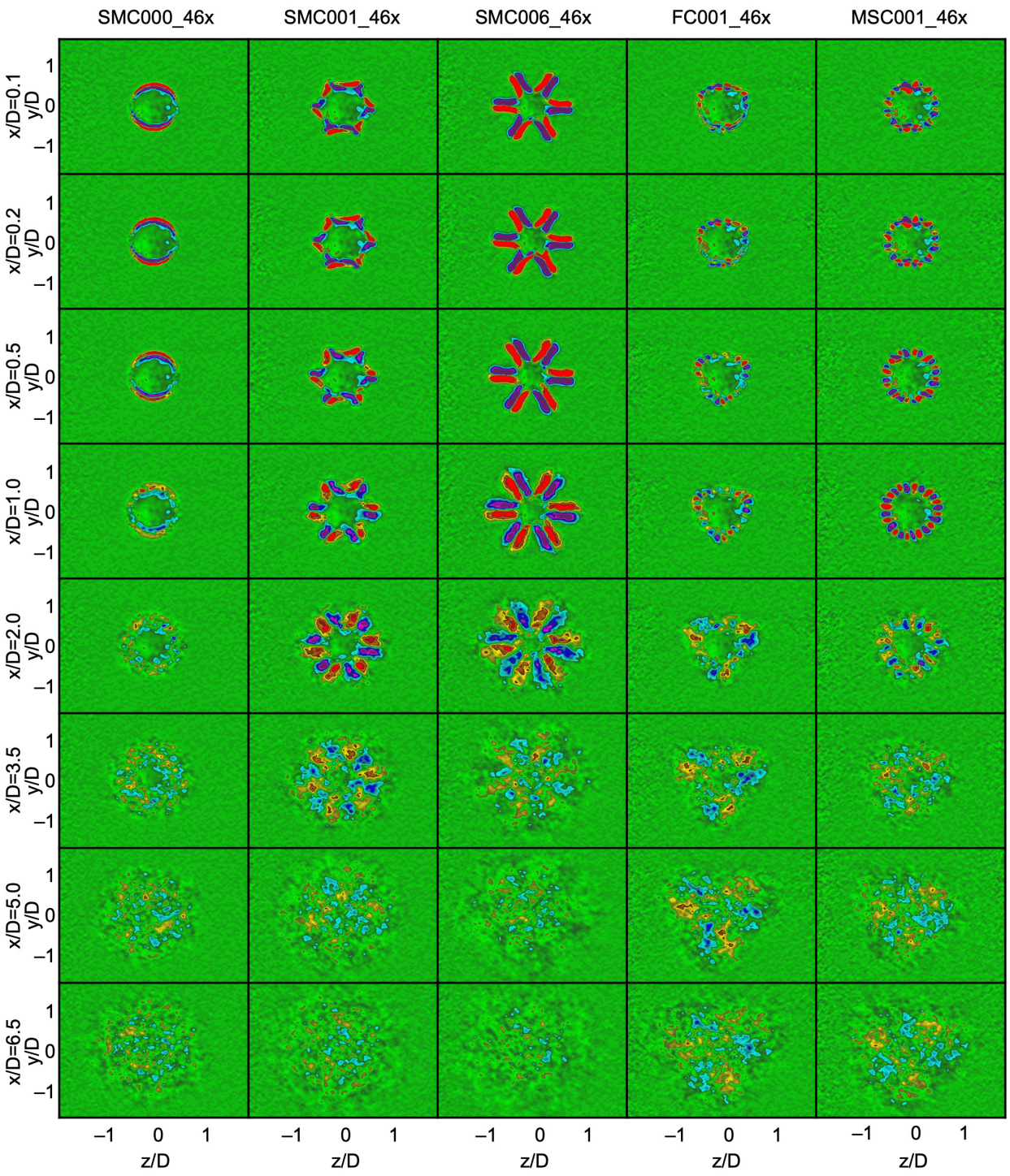

Figure 23.—Axial vorticity for SMC, FC, and MSC nozzles at Set Point 46.

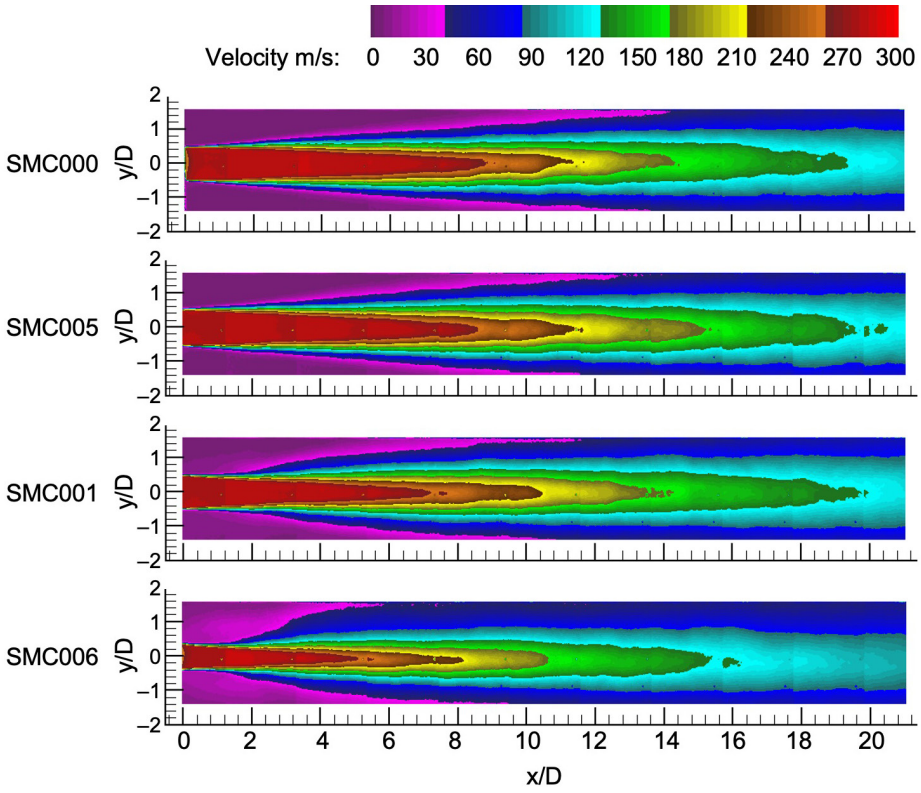

Figure 24.—Axial-plane mean velocity fields along jet-axis centerlines for M_a = 0.9 and T_r = 0.84 (Set Point 7).

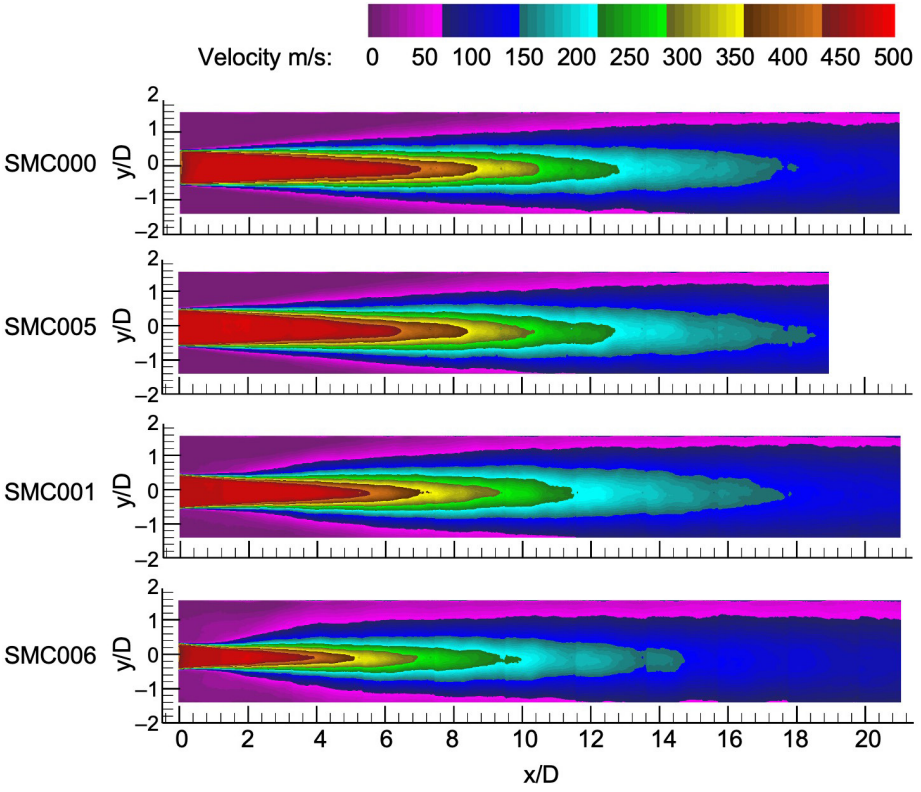

Figure 25.—Axial-plane mean velocity fields along jet-axis centerlines for M_a = 1.5 and T_r = 2.7 (Set Point 49).

5.0 Conclusions

Using a parametric family of single-flow chevron nozzles, the relationships between several simple geometric parameters and flow characteristics have been examined using SPIV. Sixteen nozzle models were included in the test program, with varying levels of chevron count, length and penetration. It was determined that chevron penetration has a major impact on both the decay of centerline jet velocities as well as mixing enhancement, over several Set Points consistent with gas-turbine engine operation.

The operating conditions included both hot and cold test points, permitting the examination of the flow behavior variation with temperature. Although the general flow characteristics of the hot jets differ systematically from the cold jets, the overall trends with chevron parameters appear the same. This appears to permit chevron jet flow measurements obtained using SPIV at Set Point 7 (cold) run conditions to be interpreted at similar operating conditions at elevated temperatures.

The SPIV measurements providing the most information from the chevron nozzle type flows considered in this test program were those generated from the cross-flow setup configuration. This particular SPIV configuration has more difficulties associated with its setup than a corresponding 2D or 3D axial-flow measurement configuration, and some measurement accuracy must be sacrificed for its implementation. However, it has been shown that the technique can be successfully applied to the types of nozzle flows produced by these chevrons, and it provides the most efficient means (facility run times) of obtaining important aeroacoustic measurement quantities, i.e., axial vorticity. Furthermore, processing techniques are available that have been shown to address some of the problems inherent in the setup, and to provide some notable improvements.

References

1. Arakeri, V.H., Krothapalli, A., Siddavaram, V., Alkislar, M.B., and Lourenco, L.M., "On the Use of Microjets to Suppress Turbulence in a Mach 0.9 Axisymmetric Jet," *J. Fluid Mech.*, vol. 490, pp. 75–98, 2003. https://doi.org/10.1017/S0022112003005202
2. Zaman, K.B.M.Q., Reeder, M.F., and Samimy, M., "Control of an Axisymmetric Jet Using Vortex Generators," *Physics of Fluids*, vol. 6, no. 2, pp. 778–793, Feb. 1994. https://doi.org/10.1063/1.868316
3. Samimy, M., Zaman, K.B.M.Q., and Reeder, M.F., "Effect of Tabs on the Flow and Noise Field of an Axisymmetric Jet," *AIAA Journal*, vol. 31, no. 4, pp. 609–619, April 1993. https://doi.org/10.2514/3.11594
4. Martens, S., "Jet Noise Reduction Technology Development at GE Aircraft Engines," ICAS 2002 Congress, Paper No. 842, 2002.
5. Saiyed, N.H., Mikkelsen, K.L., and Bridges, J.E., "Acoustics and Thrust of Separate-Flow Exhaust Nozzles With Mixing Devices for High-Bypass-Ratio Engines," AIAA Paper No. 2000-1961, 2000. https://doi.org/10.2514/6.2000-1961
6. Thomas, R.H., Choudhari, M.M., and Joslin, R.D., "Flow and Noise Control: Review and Assessment of Future Directions," NASA/TM-2002-211631, 2002. https://ntrs.nasa.gov/citations/20020045525
7. Seiner, J.M., Ukeiley, L., and Ponton, M.K., "Jet Noise Source Measurements using PIV," AIAA Paper No. 99-1869, 1999. https://doi.org/10.2514/6.1999-1869
8. Seiner, J.M., Ukeiley, L.S., and Ponton, M.K., "Jet Turbulence Measurements of Aeroacoustic Source Using Stereo PIV," AIAA Paper No. 2001-2184, 2001. https://doi.org/10.2514/6.2001-2184

9. Alkislar, M.B., Lourenco, L.M., and Krothapalli, A., "Stereoscopic PIV Measurements of a Screeching Supersonic Jet," *Journal of Visualization*, vol. 3, no. 2, pp. 135–143, 2000. https://doi.org/10.1007/BF03182406
10. Opalski, A.B., Wernet, M.P., and Bridges, J.E., "Chevron Nozzle Performance Characterization UsingStereoscopic DPIV," AIAA Paper No. 2005-444, 2005. https://doi.org/10.2514/6.2005-444
11. Bridges, J. and Wernet, M.P., "Measurements of the Aeroacoustic Sound Source in Hot Jets," AIAA Paper No. 2003-3130, 2003. https://doi.org/10.2514/6.2003-3130
12. Bridges, J. and Brown, C.A., "Parametric Testing of Chevrons on Single Flow Hot Jets," AIAA Paper No. 2004-2824, 2004. https://doi.org/10.2514/6.2004-2824
13. Bridges, J. and Wernet, M.P., "Cross-Stream PIV Measurements of Jets With Internal Lobed Mixers," AIAA Paper No. 2004-2896, 2004. https://doi.org/10.2514/6.2004-2896
14. Wernet, M.P., "Fuzzy Logic Enhanced Digital PIV Processing Software," NASA/TM-1999-209274, 1999. https://ntrs.nasa.gov/citations/19990094051
15. Wernet, M.P., "Symmetric Phase Only Filtering: a New Paradigm for DPIV Data Processing," Meas. Sci. Technol., vol. 16, no. 3, 2005, pp. 601–618. https://doi.org/10.1088/0957-0233/16/3/001
16. Taylor, J.R., *An Introduction to Error Analysis*, University Science Books, Oxford University Press, Mill Valley, CA, 1982.
17. Wernet, M.P. and Hadley, J.A., "A High Temperature Seeding Technique for Particle Image Velocimetry," *Meas. Sci. Technol.*, vol. 27, no. 12, 2016. https://doi.org/10.1088/0957-0233/27/12/125201
18. Tanna, H.K., Dean, P.D., and Fisher, M.J., "The Influence of Temperature on Shock-Free Supersonic Jet Noise," *Journal of Sound and Vibration*, vol. 39, no. 4, pp. 429–460, 1975. https://doi.org/10.1016/S0022-460X(75)80026-5